Dual Functions of Highly Potent Graphene Derivative–Poly-L-Lysine Composites To Inhibit Bacteria and Support Human Cells

Surajit Some,[†] Seok-Man Ho,[‡,⊥] Pooja Dua,[§,⊥] Eunhee Hwang,[†] Young Hun Shin,[†] HeeJoun Yoo,[†] Jong-Sun Kang,[‡] Dong-ki Lee,[§] and Hyoyoung Lee[†,*]

[†]National Creative Research Initiative, Center for Smart Molecular Memory, Department of Chemistry, Samsung-SKKU Graphene Center, [‡]Stem Cell Differentiation Laboratory, Department of Molecular and Cellular Biology, School of Medicine, and [§]Global Research Laboratory for RNAi Medicine, Department of Chemistry, Sungkyunkwan University, 300 Cheoncheon-Dong, Jangan-Gu, Suwon, Gyeonggi-Do 440-746, Republic of Korea. [⊥]These authors contributed equally to this work.

ABSTRACT

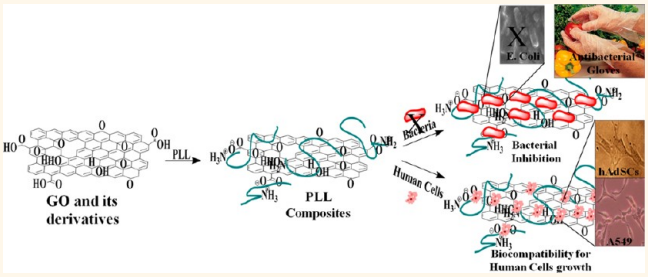

Dual-function poly(L-lysine) (PLL) composites that function as antibacterial agents and promote the growth of human cell culture have been sought by researchers for a long period. In this paper, we report the preparation of new graphene derivative–PLL composites *via* electrostatic interactions and covalent bonding between graphene derivatives and PLL. The resulting composites were characterized by infrared spectroscopy, scanning electron microscopy, and X-ray photoelectron spectroscopy. The novel dual function of PLL composites, specifically antibacterial activity and biocompatibility with human cells [human adipose-derived stem cells and non-small-cell lung carcinoma cells (A549)], was carefully investigated. Graphene–DS–PLL composites composed of 4-carboxylic acid benzene diazonium salt (DS) generated more anionic carboxylic acid groups to bind to cationic PLLs, forming the most potent antibacterial agent among PLL and PLL composites with high biocompatibility with human cell culture. This dual functionality can be used to inhibit bacterial growth while enhancing human cell growth.

KEYWORDS: PLL–graphene composite · bacterial inhibition · noncytotoxic effect · electrostatic interactions · graphene oxide

Graphene is a single-atom-thick sheet of hexagonally arrayed sp^2-bonded carbon atoms that has attracted a considerable amount of interest due to its unique physical properties.[1] This material can be used in the biomedical field[2] as biosensors,[3] biochips,[4] diagnostic devices,[5] implantable medical devices (*e.g.*, prostheses),[6] drug delivery systems,[7] and imaging probes.[8] Graphene oxide (GO) and its derivatives contain a range of reactive oxygen functional groups that facilitate their use in bioengineering. The solubility of GO and its derivatives in solvents, especially water, is required for bioengineering applications. The maximum solubility of these materials in solvent depends on both solvent polarity and the extent of surface functionalization. Recent reports have shown that GO and its derivatives are superior biocompatible materials that promote the growth of human and mammalian cells with limited or no cytotoxicity. These unique characteristics have motivated research groups to use these materials in tissue engineering, tissue implants, wound therapy, and drug delivery applications. Recently, several groups have reported that GO promotes the adhesion and proliferation of L-929 cells,[9] osteoblasts,[10] kidney cells,[11] and embryonic cells.[11] In addition, GO materials were determined to be biocompatible with mammalian cells by promoting cell adhesion and proliferation as effectively as commercial polystyrene tissue culture materials.[9] Ruiz *et al.* demonstrated that GO does not have intrinsic antibacterial, bacteriostatic, or cytotoxic properties in either bacteria or mammalian cells.[12] However, silver-coated GO films were able to produce clearing zones and induce bacterial cell death. Silver is cytotoxic in cell cultures.[13]

Poly(L-lysine) (PLL) is a polycationic homopolymer of the naturally occurring peptide L-lysine. PLL is often used for attaching and immobilizing cells to glass substrates. Bao *et al.* reported the reduced toxicity of single-walled carbon nanotube (SWNT) networks processed on surfaces

* Address correspondence to hyoyoung@skku.edu.

Received for review May 19, 2012 and accepted July 30, 2012.

Published online July 30, 2012
10.1021/nn302215y

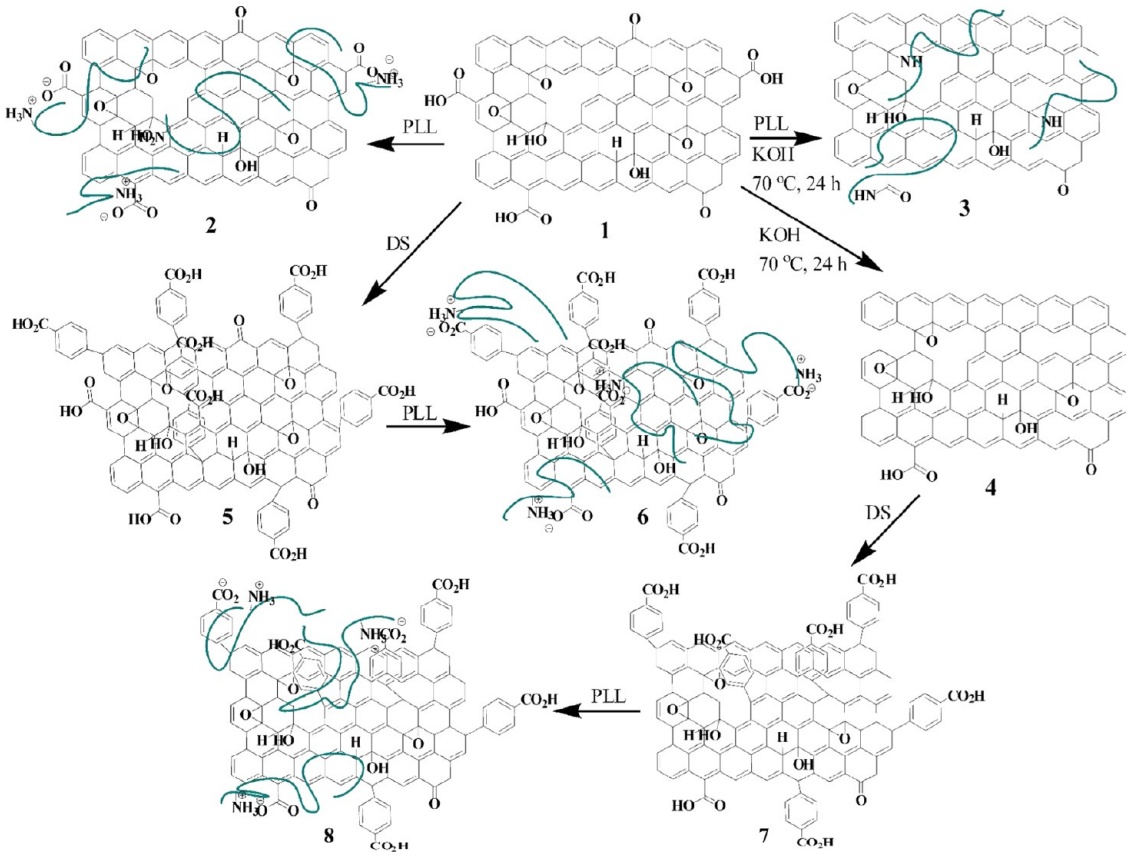

Scheme 1. Schematic diagram of the preparation of various composites synthesised from graphene oxide. 1, GO; 2, GO−PLL; 3, rGO−PLL; 4, rGO, 5, GO−DS; 6, GO−DS−PLL; 7, rGO−DS; and 8, rGO−DS−PLL.

functionalized with PLL.[14] In addition, the antimicrobial activity of PLL has been well-established.[15] On the basis of these observations, we speculated that PLL had antimicrobial activity and was biocompatible with cells by promoting cell adhesion and proliferation.

The main goal of this study was to prepare a variety of PLL composites with potent antibacterial activity and high biocompatibility in cell culture. The growth of bacteria (*Escherichia coli*) and human cells (adipose-derived stem cells and lung cancer cells) in the presence of graphene oxides and their PLL composites was determined by evaluating cell growth and antimicrobial activity. A previous report[14] suggested that the amine functional group and GO could be extended to biopolymers containing amine moieties to enable adsorption onto GO and its derivatives for biocompatibility and increased antibacterial activity.[16] However, no report has demonstrated that graphene derivative−PLL composites have intrinsic antibacterial properties with biocompatibility in cell cultures.

In this paper, we report a new, easy method to quickly prepare graphene derivative−PLL composites in which PLL is electrostatically and covalently bonded to the surfaces of GO and its derivatives. We also determined how to increase the number of carboxylic acid functional groups on the surface of GO and reduced graphene oxide (rGO) using 4-carboxy benzene diazonium salt (DS) to attach more PLL molecules to the surface of composites (Scheme 1). We hypothesized that an increase in the number of carboxylic acid groups on the surface of GO/rGO should lead to the attachment of more PLL, producing GO/rGO−DS−PLL composites with increased antibacterial activity. The use of natural polycationic biopolymers could improve the biocompatibility and antibacterial activity of GO and its derivatives. Furthermore, we hypothesized that PLL composite materials would effectively inhibit microbial proliferation and promote human cell proliferation, demonstrating that PLL composites exhibit antibacterial activity and are general growth enhancers by acting as a scaffold for cell surface attachment and proliferation.

RESULTS AND DISCUSSION

Characterization of Graphene Derivative−PLL Composites. All of the materials were characterized by Fourier transform infrared spectroscopy (FT-IR), X-ray photoelectron spectroscopy (XPS), and scanning electron microscopy (SEM) analyses. We prepared different PLL composites by chemical and physical bonding. Using FT-IR spectroscopy (Figure 1), the characteristic absorption of different PLL functional groups on GO and its derivatives was determined. The presence of PLL physically attached to graphene oxide and its

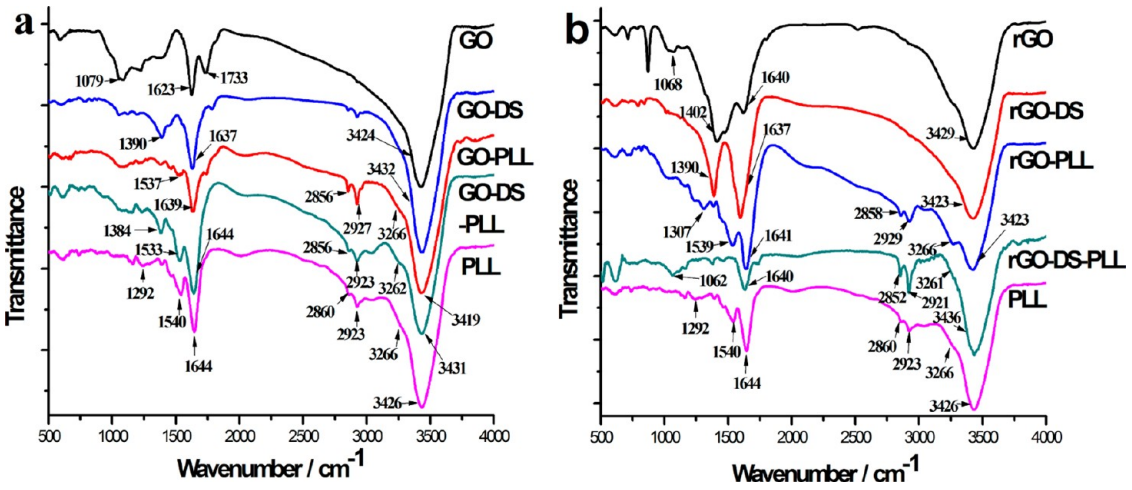

Figure 1. FT-IR spectra of different compounds. (a) FT-IR spectra of GO, GO−DS, GO−PLL, GO−DS−PLL composites and PLL. (b) FT-IR spectra of rGO, rGO−DS, rGO−PLL, rGO−DS−PLL composites and PLL.

derivatives by electrostatic interactions was confirmed by FT-IR. The spectrum in Figure 1a shows the different types of oxygen functionalities in graphene oxide at 3424 (O−H stretching vibrations), 1733 (C═O stretching vibrations), 1623 (C═C skeletal vibrations from unoxidized graphitic diamonds), and 1079 cm^{-1} (C−O stretching vibrations).[17] After reacting GO with the DS precursor to produce the GO−DS derivative, the appearance of peaks at 3432 (O−H stretching vibrations) and 1637 cm^{-1} (C═O stretching vibrations) indicated that these GOs were functionalized with more carboxylic acid groups.[18] The spectra of GO−PLL exhibited characteristic PLL absorption features at 3266 cm^{-1} (N−H stretching vibrations in free NH_3^+ groups) and 1639 cm^{-1} (C═O stretching vibrations). Peaks at 2856 and 2927 cm^{-1} (CH_2 stretching vibrations) also appeared in the GO−PLL sample.[19] FT-IR spectra of GO−DS−PLL also displayed significant PLL peaks at 3262 (N−H stretching vibrations in free NH_3^+ groups), 1644 (C═O stretching vibrations), and 2856 and 2923 cm^{-1} (CH_2 stretching vibrations).[20] These results demonstrate that PLL was successfully grafted onto GO and its derivative (GO−DS).

PLL was confirmed to be attached to rGO and its derivatives *via* covalent and electrostatic interactions by FT-IR spectra (Figure 1b). In the as-prepared rGO, we observed peaks at 3429 (O−H stretching vibrations), 1640 (C═O stretching vibrations), and 1402 cm^{-1} (C−C skeletal vibrations from unoxidized graphitic diamonds). When rGO was functionalized with more oxygen groups *via* reactions with the DS precursor, significant peaks appeared at 3423 (O−H stretching vibrations) and 1637 cm^{-1} (C═O stretching vibrations), indicating the formation of the rGO−DS composite (Figure 1b). FT-IR spectra of the rGO−PLL composite revealed peaks at 3266 (N−H stretching vibrations), 1641 (C═O stretching vibrations), and 2856 and 2929 cm^{-1} (CH_2 stretching vibrations), which appeared to be due to PLL in the composite.[20] FT-IR spectra of rGO−DS−PLL also revealed peaks at 3266 and 1640 cm^{-1}, which corresponded to N−H stretching vibrations in free NH_3^+ groups and C═O stretching vibrations, respectively. The CH_2 stretching vibrations at 2856 and 2929 cm^{-1} also appeared to be due to PLL in the composite.

The formation of PLL composites was also confirmed by XPS analysis (Figure 2), which is an effective tool used to characterize the presence of different elements, such as C, N, and O. On the basis of XPS analyses, the as-prepared GO had a low C/O ratio (2.2). After treating GO with PLL in the presence of KOH at 70 °C for 24 h, the C/O ratio gradually increased to 3.5, while a significant decrease in the oxygen atomic percentage occurred by forming a covalent bond with PLL. Notably, there was no N present in the initial GO. However, a noticeable amount of N (9.5%) was present in the as-prepared sample. XPS analysis revealed that N atoms were incorporated in the as-prepared rGO−PLL sample *via* covalently bonded PLL. For control experiments, we prepared an rGO sample by reducing the as-prepared GO with KOH at 70 °C for 24 h without PLL. The high-resolution C1s XPS spectrum of the control rGO sheets displayed a sharp peak at 284.6 eV, corresponding to C−C bonds in a conjugated honeycomb lattice, and peaks at 286.6, 287.9, and 288.9 eV, which are due to the different C−O bonding configurations that result from the harsh oxidation and destruction of the sp^2 atomic structure of graphite (Figure 2e).[21] The rGO−PLL composite exhibited a peak at 286.2 eV by peak fitting, suggesting bond formation between carbon and nitrogen (C−N), which overlaps with C−O bonding energy (Figure 3f).[22] The peak at 287.7 represents C(O)−N bonding energy, which also overlaps with C═O bond energy.[22] These experimental findings suggest that certain oxygen functional groups in the as-prepared GO were involved in reactions with PLL to form C−N and C(O)−N bonds, forming an rGO−PLL composite. The bonding configurations of the N atoms

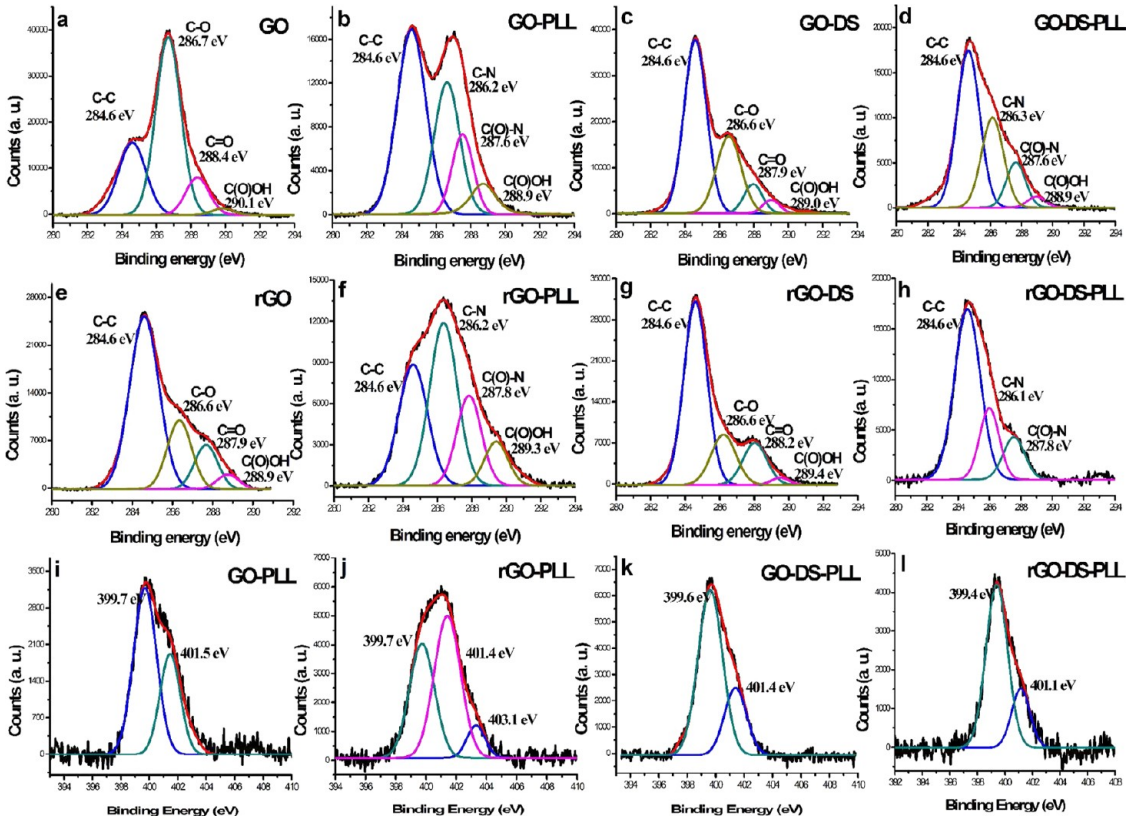

Figure 2. XPS spectroscopy of all of the compounds. High-resolution C1s spectra of (a) GO, (b) GO−PLL composite, (c) GO−DS composite, (d) GO−DS−PLL composite, (e) rGO, (f) rGO−PLL composite, (g) rGO−DS composite, and (h) rGO−DS−PLL composite. High-resolution N1s spectra of (i) GO−PLL, (j) rGO−PLL, (k) GO−DS−PLL, and (l) rGO−DS−PLL composite.

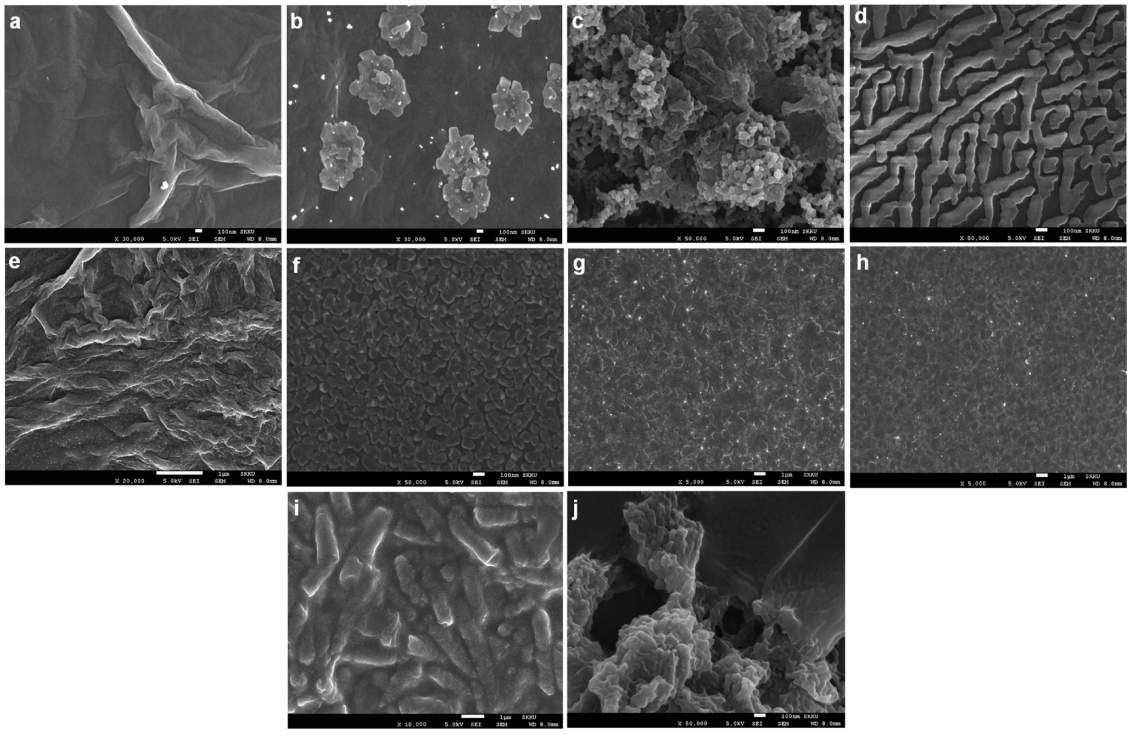

Figure 3. SEM images of different materials. SEM images of (a) GO, (b) GO−PLL composite, (c) rGO−PLL composite, (d) as-prepared rGO, (e) GO−DS composite, (f) rGO−DS composite, (g) GO−DS−PLL composite, (h) rGO−DS−PLL composite, (i) bacterial biofilm containing GO after 12 h, and (j) rGO−PLL composite with no bacterial biofilm after 12 h.

in rGO–PLL composites were determined based on high-resolution N1s XPS spectra. The peaks at 399.7, 401.4, and 403.1 eV correspond to nitrogen atoms in amine moieties, a quaternary or protonated nitrogen, and oxidized nitrogens, respectively (Figure 2j).[23]

GO and control rGO samples were treated with the DS precursor to prepare GO–DS and rGO–DS composites with more carboxylic acid groups. XPS analyses revealed that the C/O ratio of GO–DS and rGO–DS (3.4 and 3.9) was increased compared with GO and rGO. On the basis of the high-resolution C1s XPS spectra, the peak percentage of C═O and C(O)OH bonds was increased with respect to C–O in comparison with GO and rGO samples. Thus, these results suggest that GO and rGO were well-functionalized with additional carboxylic acid groups. We prepared the GO–PLL composite *via* the physical absorption of PLL onto the GO surface using the formation of electrostatic interactions between the functional groups of GO and PLL. XPS analyses revealed that the C/O ratio (3.0) was increased compared with GO. A peak corresponding to C–N bonding energy appeared at 286.2 eV, representing C(O)–N bonding energy at 287.6 eV (Figure 2b). The bonding configurations of N atoms in GO–PLL composites were determined based on high-resolution N1s XPS spectra. Notably, the initial GO lacked nitrogen, and a noticeable amount of N (10.6%) was present in the as-prepared sample. We determined that there were two types of C–N binding energy: the peaks at 399.7 and 401.5 eV were attributed to the nitrogen atoms of amine moieties and quaternary or protonated nitrogens, respectively (Figure 2i).[23]

Finally, we prepared GO–DS–PLL and rGO–DS–PLL composites *via* the physical absorption of PLL onto the surface of GO–DS and rGO–DS composites using electrostatic interactions. XPS analyses revealed that the C/O ratios of GO–DS–PLL and rGO–DS–PLL (4.7 and 5.6) were increased compared with GO–DS and rGO–DS composites (3.4 and 3.9), respectively. According to high-resolution C1s XPS spectra, the second and third highest peak intensities of GO–DS–PLL and rGO–DS–PLL, which represent the C–N and C(O)–N binding energies, were higher than those of the initial GO–DS and rGO–DS composites. The bonding configurations of N atoms in GO–DS–PLL and rGO–DS–PLL were determined based on high-resolution N1s XPS spectra. There was no nitrogen in the initial GO–DS and rGO–DS. However, a noticeable amount of N (11.9 and 11.7% for GO–DS and rGO–DS, respectively) was present in the as-prepared samples. In both cases, we determined that the peaks at 399.6 and 399.4 eV were attributed to the nitrogen atoms in amine groups and those at 401.4 and 401.1 eV corresponded to quaternary or protonated nitrogen (Figure 2k,l).[23] These experimental findings suggest that oxygen functional groups in as-prepared GO, GO–DS, and rGO–DS are involved in forming electrostatic interactions with PLL to form their corresponding composites.

Scanning electron microscopy (SEM) analysis was used to determine the surface morphology of various GO derivatives (Figure 3). We observed thin and wrinkled GO sheets in the SEM images of GOs (Figure 3a). PLL physically attached to GO surfaces was shown in SEM images of GO–PLL. The SEM image of the GO–PLL composite showed that PLL molecules were absorbed onto the surface of wrinkled GO sheets in the arrangement of a flower (Figure 3b). An rGO–PLL composite was formed by reacting GO and PLL under KOH at 70 °C for 24 h. The SEM image of the rGO–PLL composite (Figure 3c) showed that the PLL composite formed on the rGO. We also observed differences in the SEM image compared with control rGO and PLL samples (Figure 3d and Supporting Information Figure 1S). GO–DS (GO reacted with the DS precursor) exhibited a more wrinkled morphology compared with as-prepared GO (Figure 3e), whereas rGO–DS produced smaller sheets compared with rGO (Figure 3f). The SEM images of GO–DS–PLL and rGO–DS–PLL composites showed that PLL molecules were physically attached to the surface of GO–DS and rGO–DS composites, respectively (Figure 3g,h).

Bacterial Proliferation in the Presence of GO and Various PLL Composites. To determine the effect of various GO, rGO, and PLL composites on bacterial growth, samples containing 5 mL of Luria–Bertani (LB) nutrient broth in 20 mL test tubes were incubated with PLL composites to a final concentration of 25 μg/mL. Samples were then inoculated with *E. coli* bacterial cells to a 0.01 optical density (OD).[12] Experiments were performed with the same dose of compounds **1**–**8** (Scheme 1), including PLL. The experimental control was prepared by inoculating *E. coli* to an OD of 0.01 in 5 mL of LB broth without any of the composites. We examined the supernatant at various times to evaluate the growth of *E. coli* without disturbing the precipitate at the bottom of each sample containing different composites. At 3, 6, 9, and 12 h, we determined the bacterial growth by measuring the absorbance of cultures at 600 nm.

The ODs of PLL composites (compounds **2**, **3**, **6**, and **8**) and PLL only did not increase after 3 h, whereas the ODs of the other samples (composites without PLL) significantly increased compared with control samples (*i.e.*, without bacteria). In samples containing rGO–PLL and PLL, the ODs increased after 6 h compared with control samples. However, the ODs were still lower than samples containing only bacteria. Culture tubes containing GO–PLL (compound **2**), GO–DS–PLL (compound **6**), and rGO–DS–PLL (compound **8**) did not have any distinguishable difference in ODs compared with control samples (Figure 4). The ODs of rGO–PLL and PLL became saturated and then decreased, which is a normal phenomenon of *E. coli*. Surprisingly, samples containing GO–PLL (compound **2**), GO–DS–PLL (compound **6**), and rGO–DS–PLL (compound **8**) did not show any

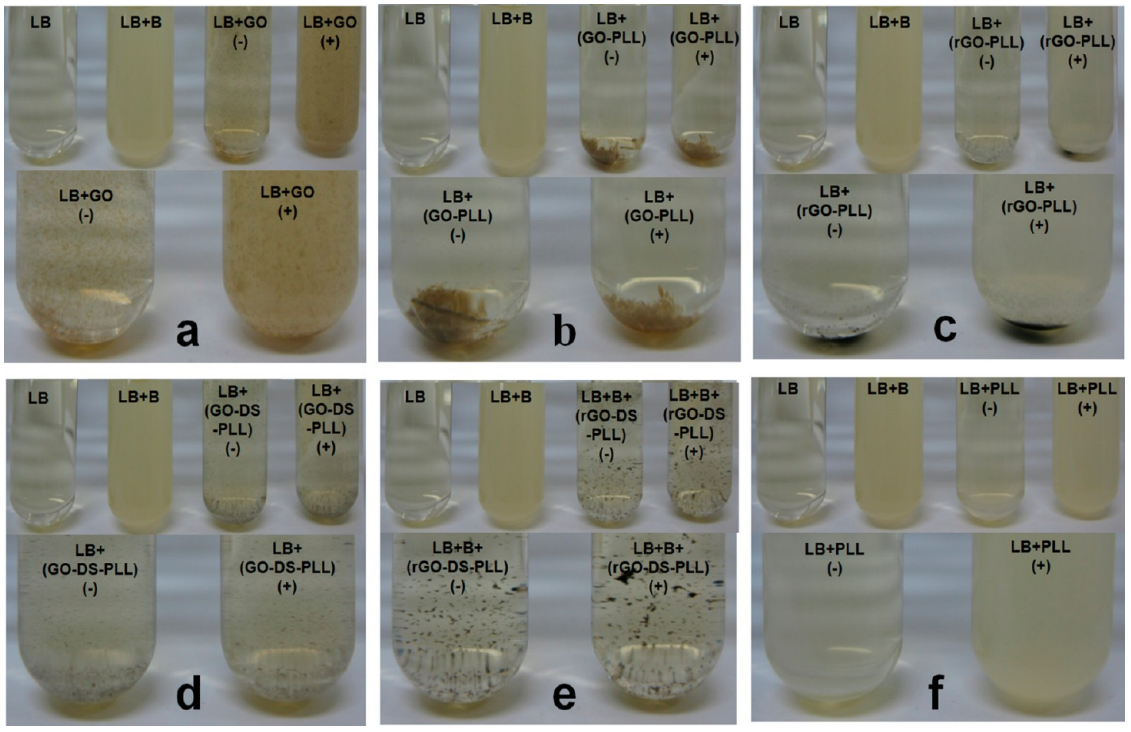

Figure 4. Bacterial proliferation in the presence of various as-prepared composites. Bacterial growth in four test tubes containing the following components after 9 h: LB, LB + E. coli, LB + composites, and LB + composites + E. coli. The materials used were (a) GO, (b) GO−PLL, (c) rGO−PLL, (d) GO−DS−PLL, (e) rGO−DS−PLL, and (f) PLL.

noticeable difference in ODs (average absorbance in the range of 0.00−0.03) after 12 h compared with the controls. The ODs of GO and other composites (without PLL) gradually increased over time and became saturated compared with controls. After 9 h, samples containing bacteria appeared to be more turbid and had the highest ODs (average absorbance of 2.345), which may represent a saturation point in comparison with control samples (except samples **2**, **6**, and **8**; Figures 4 and 5a and Supporting Information Figure 2S).

The plot of ODs shown in Figure 5a indicates that the bacterial inhibition of GO−PLL, GO−DS−PLL, and rGO−DS−PLL was much higher than PLL alone. The bacterial inhibition of rGO−PLL, which differed from other PLL composites, was not effective compared with GO−PLL, GO−DS−PLL, and rGO−DS−PLL. PLL in the rGO−PLL composite was covalently bonded to the rGO surface, forming a less charged composite compared with other PLL composites. Previous studies have shown that when a colloidal suspension of GO in water is added to a media solution containing salts, GO aggregates, and precipitates out of the suspension, producing low-density aggregates.[12,24] The presence of a large amount of cells in biofilms has also been reported, indicating that colloidal GO has a direct effect on bacterial proliferation when added to liquid media.[12] After 12 h, bacterial growth on precipitated GO and rGO−PLL samples was analyzed by SEM (Figure 3). The SEM images showed that the precipitated samples of GO were covered by a thick bacterial biofilm (Figure 3i) containing a large mass of aggregated cells compared with the control sample (LB broth and GO, Figure 3a), whereas bacterial samples with rGO−PLL did not show any biofilm formation on the surface (Figure 3j). These results indicate that the bacterial inhibition by rGO−PLL composites was not enough to prevent bacterial growth in LB broth compared with other PLL composites but did inhibit bacterial growth on the surface of the rGO−PLL composite. Thus, any type of PLL composite could act as an antibacterial agent. The ODs shown in Figure 5 demonstrate the antibacterial activity of PLL composites. GO−DS−PLL and rGO−DS−PLL composites were the most effective inhibitors of bacterial growth and were more potent than GO−PLL composites. GO−PLL, GO−DS−PLL, and rGO−DS−PLL composites were more potent inhibitors than PLL and rGO−PLL. PLL is electrostatically adsorbed to the cell surface of bacteria and then strips the outer membrane of the bacteria cell, which can eventually lead to the abnormal distribution of the cytoplasm and cause cell damage.[25] Because PLL is a cationic polymer, PLL in GO−PLL, GO−DS−PLL, and rGO−DS−PLL composites was attached to the anionic carboxylate groups of GO, GO−DS, and rGO−DS with a high surface area *via* electrostatic interactions. Thus, more anionic carboxylate groups attached to 2D nanomaterial with a high surface area can lead to the attachment of more cationic PLL polymer, increasing bacterial inhibition compared with PLL, which does not have a high surface area. However, we hypothesized that the amount of PLL attached to the rGO surface *via* covalent bonding should be less than

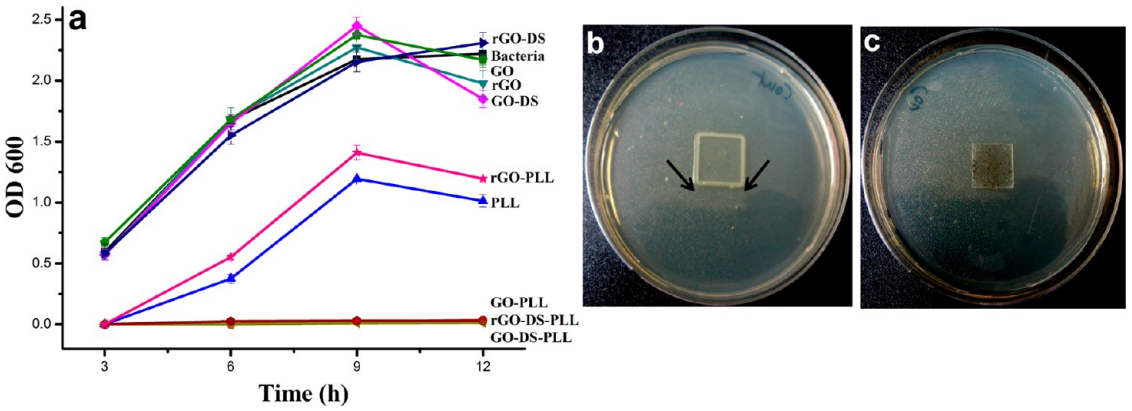

Figure 5. OD plot of bacterial growth on solid surfaces. (a) Graphs showing bacterial growth levels in the supernatant of samples containing as-prepared composites. (b) PET and (c) PLL composite coated on PET inoculated with E. coli and cultured at 37 °C for 24 h.

electrostatically attached PLL composites, resulting in lower bacterial inhibition. Indeed, our experimental results demonstrated that GO and rGO functionalized with more carboxylic acid groups provided more PLL-attached composites, indicating that these composites are better antibacterial agents (Figure 5).

To further see if the graphene derivative–PLL composites besides causing growth inhibition also have bactericidal properties, we performed a live/dead assay with the GO–DS–PLL composite. The *E. coli* were cultured in 1 mL of Luria–Bertani (LB) nutrient broth in 5 mL test tubes until it reached an OD of 0.1 (3×10^7 cells). The bacterial cells were then incubated for 1 h with the GO–DS–PLL composites to a final concentration of 25 μg/mL. After that, SYTO 9 and propidium iodide (PI) dye were used to perform the live/dead assay. Since only living and dead bacteria are getting stained by SYTO 9 or PI, bacteria can easily be spotted and localized between abiotic particles. The positively charged fluorescent label PI can only stain dead bacterial cells since it cannot pass through the positive charged cell membranes of living cells. In contrast to the PI molecules, the neutral SYTO 9 molecules can pass through the cell membrane of both living and dead cells. Nevertheless, in the case of labeling dead cells with a mix of SYTO 9 and PI, the green fluorescence caused by SYTO 9 will be suppressed by a fluorescence resonance energy transfer (FRET) effect and dead cells fluoresce in the red. It is well-known that the combination of SYTO 9 and PI is well-suited for staining eukaryotic cells.[26] In Figure 6S, the staining results for all analyzed species are presented. The SYTO 9 and PI overlay image in Figure S6c clearly shows the presence of only live cells in control, and Figure S6d shows the presence of only dead cells on composites. The relative average intensity of dead cells for each condition was calculated to be 4 and 97% for the control and the GO–DS–PLL-treated sample, respectively (Supporting Information Figure 7S). The data were quantified by taking the ratio of the number of dead cells to the total number of cells for the two conditions, the control and the GO–DS–PLL treated samples ($n = 3$). The differences between the percentages for the control and the material-coated samples were found to be statistically significant using a t test ($p < 0.005$). This live/dead assay experiment showed that the GO–DS–PLL composite had bactericidal activity in addition to antibacterial activity on *E. coli* cells.

To explore potential applications of PLL composites, a bacteria-free plastic glove was fabricated with one of the most potent GO–DS–PLL composite. To determine the antibacterial activity of the PLL composite on the plastic solid surface, the pre-plasma-treated polyethylene terephthalate (PET) film was coated with the GO–DS–PLL composite by spin-casting 250 μL of the GO–DS–PLL composite solution (1 mg/mL). The GO–DS–PLL composite on the PET substrate was allowed to dry and then inoculated with bacteria by submerging the film in a solution containing *E. coli* (4×10^8 cells/mL) for 1 min. PET film without the GO–DS–PLL composite served as a control. The resulting PET films were then recovered, dried, placed on a sterile LB culture plate, and incubated for 24 h at 37 °C. One side of PET film coated with a PLL composite was placed in contact with a sterile LB culture plate, as shown in Figure 5b,c. Large bacterial colonies were observed around the edges of the PET film (Figure 5b). No bacterial growth was observed in the PLL-coated PET sample (Figure 5c). These results indicate that a large amount of bacteria grew to the edge of the PET film in the PET sample, whereas the PLL composite-coated PET showed inhibited bacterial growth. Thus, antibacterial plastic gloves can be prepared using GO–DS–PLL composites, which can be efficiently attached to the hydrophilic PET surface.

Human Cell Attachment to and Proliferation on PLL Composite Films. We evaluated the effect of composite (Scheme 1, compounds **1**, **2**, **3**, **6**, and **8**) films on human cell attachment and proliferation using human adipose-derived stem cells (hAdSCs)[27] and non-small-cell lung carcinoma (NSCLC) A549 cells.[28] Various composites

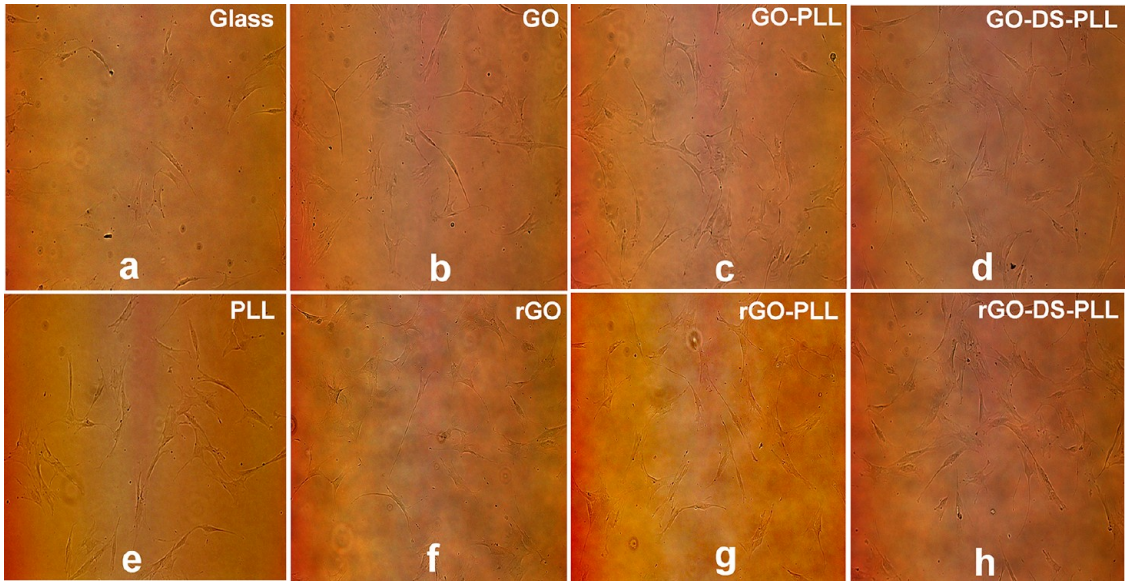

Figure 6. Growth of human adipose-derived stem cells (hAdSCs) on various PLL composites. (a) Micrographs showing hAdSC cell attachment and growth on glass coverslips. Micrographs showing hAdSC cell attachment and growth on (b) GO, (c) GO−PLL, (d) GO−DS−PLL, (e) PLL, (f) rGO, (g) rGO−PLL, and (h) rGO−DS−PLL.

were coated on glass coverslips by spin-casting samples with 100 μL of a 1 mg/mL solution.

Control glass coverslips and GO/rGO composite-coated coverslips were placed in a culture dish followed by the addition of culture media and various cells. Cells were allowed to attach and grow on the coverslips. Cell attachment was assessed by light microscopy at different times. Representative images of different cell morphologies of hAdSCs and A549 cells after incubation for 24 and 36 h, respectively, are shown in Figures 6 and 7. The results indicate that both human cells efficiently attached to and grew on glass coverslips coated with composites (Figures 6 and 7). Both types of human cells attached to PLL composite-coated coverslips at higher levels compared with coverslips coated with only GO[12] or PLL. The attachment and growth of human cells on rGO−PLL composites (Figure 7g) were lower compared with GO−PLL (Figure 7c), GO−DS−PLL (Figure 7d), and rGO−DS−PLL (Figure 7h) composites. The micrographs of A549 cells showed marked morphological changes, cell enlargement, and spreading on coverslips coated with composites compared with control glass coverslips (Figure 7a), which is characteristic of effective cell attachment and cell growth (Figure 7). The micrographs of hAdSCs also showed noticeable morphological changes and spreading on the coverslips coated with composites compared with control glass coverslips (Figure 6). In both cases, the attachment and growth of human cells on PLL composites were much higher than coverslips coated with reported GO or PLL (Figures 6e and 7e). In control experiments with only a glass coverslip, few cells were attached, indicating a lack of enlargement and growth of hAdSCs and A549 cells (Figures 6a and 7a).

The proliferation ability of the graphene derivative−PLL composite and the only PLL-coated coverslips were tested by fluorescence staining with bromodeoxyuridine (BrdU) assay as a molecular probe. This is a common technique used to fluorescently tag a probe that is a frequently characterized parameter for a cell proliferation.[29] Nuclei were visualized by 4′,6-diamidine-2-phenylindole dihydrochloride (DAPI, Roche) staining. Thus, the number of DAPI-positive cells is equivalent to the number of total cells. BrdU is integrated into the DNA strand during DNA synthesis, which is only shown in proliferating cells. Therefore, BrdU-positive cells are equated to proliferating cells. We did this experiment on the GO−DS−PLL composite and on only PLL-coated (control) coverslip. Control sample's (only PLL-coated) cells exhibited only ∼13 and ∼11% of BrdU-positive cells, whereas ∼29 and 25% of GO−DS−PLL-coated sample cells were positive for BrdU, respectively (Figures 8S, 9S, and 10S). The data were quantified by taking the ratio of the number of proliferating cells to the total number of cells for each of two conditions, control and GO−DS−PLL-coated samples (n = 5). The differences between the percentages for the control and material-coated samples were found to be statistically significant using a t test ($p < 0.005$). These data suggested that the graphene derivative−PLL composite has more than double ability to proliferate human cells more efficiently in comparison to the only reported PLL, which implies that these materials are not cytotoxic for human cell culture with a used amount of material. These studies clearly demonstrated that the PLL composite films, beyond not exerting any cytotoxic effects on the cells, promoted an attachment and proliferation of human cells. Taken together, these results indicated that all PLL composites were a great support for human cell attachment, growth, and proliferation.

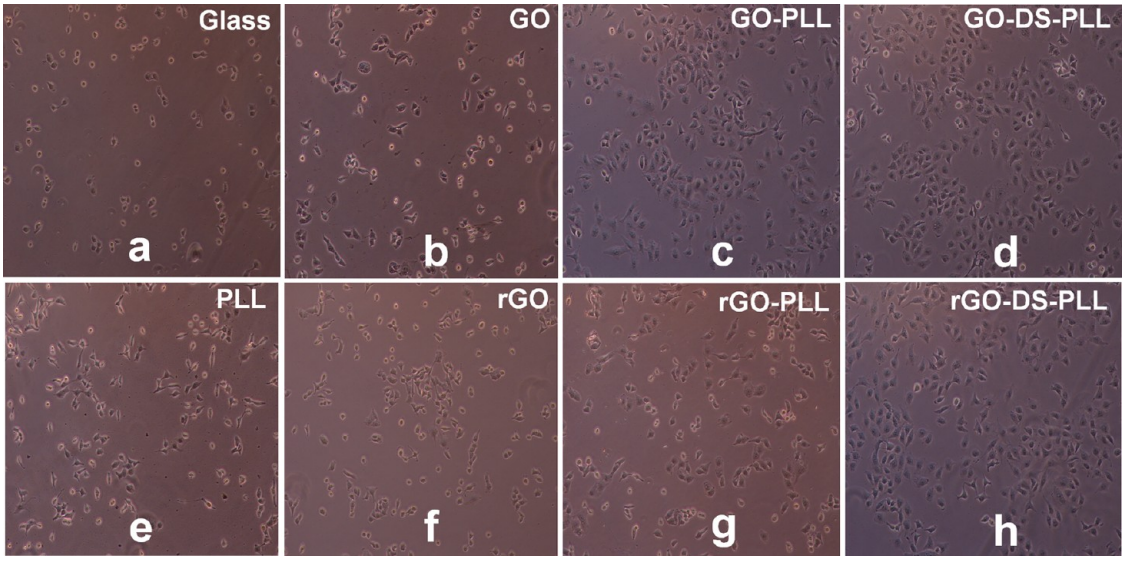

Figure 7. Human non-small-cell lung carcinoma (NSCLC) A549 cell growth on different PLL composites. Micrographs showing the attachment and growth of A549 cells on (a) glass coverslips and coverslips coated with (b) GO, (c) GO–PLL, (d) GO–DS–PLL, (e) PLL, (f) rGO, (g) rGO–PLL, and (h) rGO–DS–PLL.

It is assumed that a lot of positively charged PLL molecules are effectively attached on the negatively charged graphene surface. The surface area of those composites are very high in comparison to that of only PLL due to high surface area of graphene, and those composites showed much better performance than only PLL. As a result of positively charged high surface area, those composites can come into contact with many negatively charged bacteria at a time and show much higher affectivity than that of only PLL. They also enhance the human cell attachment and proliferation on their surfaces, compared with that of only PLL. This is the only difference in the reactivity of graphene derivative–PLL composites and only PLL, and the mechanism of reactivity of those composites is very similar to only PLL.[12,30] We also assumed that the antibacterial property of the graphene derivative–PLL composites is dominated by the electrostatic interaction between those composites and bacteria.

CONCLUSION

The study demonstrates that GO has no antibacterial properties, which is in accordance with previous reports. We synthesized novel graphene derivative–PLL composites through the electrostatic and covalent bonding of PLL to GO and rGO derivatives. GO–PLL and newly designed GO–DS–PLL and rGO–DS–PLL composites were prepared *via* electrostatic interactions between PLL and the respective starting materials. The rGO–PLL composite was synthesized by covalent bonding and had the least amount of PLL among the graphene derivative–PLL composites investigated in this study. The PLL cationic polymer generated more charges on graphene–DS–PLL composites. As a result, these composites exhibited the most potent antibacterial activity. Applications of PLL composites were explored by fabricating antibacterial plastic gloves that can protect against bacterial growth. The GO–DS–PLL composite was successfully attached to a plastic PET solid surface and exhibited antibacterial activity. In addition, GO–PLL, GO–DS–PLL, and rGO–DS–PLL composites were also shown to be cell growth enhancers by acting as scaffolds for cell surface attachment and proliferation. This is the first report demonstrating that graphene derivative–PLL composites can provide potent antibacterial activity with a noncytotoxic effect on human cell cultures. The exact mechanism of bacterial inhibition and the biocompatibility of graphene derivative–PLL composites are under investigation. The results of this study provide more insight into the biological properties of PLL composites and their potential biomedical and biotechnological applications.

METHODS

Preparation of Graphene Oxides (GOs). GO was prepared from natural graphite powder by the modified Hummers and Offenman's method using sulfuric acid, potassium permanganate, and sodium nitrate.[31]

Synthesis of GO–DS and rGO–DS Composites. GO and rGO were immersed in an H_2SO_4 solution at room temperature and sonicated for 30 min. The mixture was then poured into a flask, and 4-aminobenzoic acid and sodium nitrite were quickly added *via* a syringe. The mixture was vigorously stirred at 60 °C for 1 h.[32] Because the resulting solution was highly acidic, it was diluted with water and neutralized by NaOH (2 M). The product was then washed with water and ethanol and dried at 60 °C for 24 h in a vacuum oven.

Synthesis of GO–PLL, GO–DS–PLL, and rGO–DS–PLL Composites. GO, GO–DS, and rGO–DS nanosheets were dispersed in

deionized distilled water with four times the amount of PLL to GO, GO–DS, and rGO–DS. The reaction mixture was stirred at 4 °C for 24 h, and the mixture was subjected to ice-cold ethanol (100%) and maintained at 4 °C to facilitate precipitation overnight (18 h). The visible precipitate was subjected to centrifugation at 14 000 rpm for 30 min, and the resulting pellet was dried under vacuum. The dried pellet was dispersed in deionized distilled water by sonication (1 mg/mL).

Synthesis of rGO–PLL Composite. Generally, rGO–PLL was prepared by vigorously stirring a solution of 2 mg of GO, 8 mg of PLL, and 10 mg of KOH in 10 mL of H_2O at 70 °C for 24 h. The mixture was subjected to ice-cold ethanol (100%) and kept at 4 °C to facilitate precipitation overnight (18 h). The visible precipitate was then subjected to centrifugation at 14 000 rpm for 30 min, and the resulting pellet was dried under vacuum. The dried pellet was dispersed in deionized distilled water by sonication (1 mg/mL).

Coating of Glass Coverslips with Composite Films. A suspension of each material was obtained by sonicating the obtained composite powder in water (1 mg/mL). With a microsyringe, 100 μL of each solution was dropped onto a glass coverslip, which was spinning at 4000 rpm, for approximately 30 s. The coverslip was allowed to dry in a fume hood, and a thin film formed on the coverslip. Glass coverslips with or without composite films were placed in culture dishes (10 cm in diameter) and treated with UV radiation for 30 min.

Bacterial Cell Culture. *Escherichia coli* strain DH5α was grown in Luria–Bertani (LB) broth in 20 mL test tubes and incubated for 12 h at 37 °C and with different composites to a final concentration of 25 μg/mL.[12]

Bacterial Growth on a Solid Surface. The PET and composite-coated PET substrates were inoculated with bacteria by submerging the film in a solution containing *E. coli* (4×10^8 cells/mL) for 1 min. The resulting PET films were then recovered, dried, placed on a sterile LB culture plate, and incubated for 24 h at 37 °C.[12]

Human Cell Culture. Non-small-cell lung carcinoma (A549) cells were cultured in RPMI medium 1640 (Gibco) supplemented with 10% fetal bovine serum (FBS) and 1% antibiotics (penicillin and streptomycin). The cells were cultured at 37 °C in a humidified atmosphere with 95% air and 5% CO_2 for 48 h (reaching 70% confluence) before being subcultured. For experiments, 12×10^4 cells were seeded in a 35 mm culture dish containing the glass slides (with or without composite films) and incubated to allow the cells to attach and grow on the glass coverslips. After 36 h, the morphology of cell growth was observed under a microscope equipped with a camera.

Human Adipose-Derived Stem Cells (hAdSCs). hAdSCs were isolated from adipose tissue using previously described methods (Schaffler and Buchler, 2007). Briefly, the adipose tissue was rinsed with PBS and centrifuged at 1200*g* for 5 min. The rinsed tissue pellet was treated with 0.0075% collagenase (Type XI, Sigma-Aldrich) in PBS at 37 °C for 1 h on a shaker. Enzymatic digestion was inactivated by the addition of an equal volume of growth medium (high-glucose DMEM, 10% FBS, and 1% penicillin/streptomycin) followed by centrifugation at 1200*g* for 10 min. The pellet was resuspended in DMEM/F12 medium supplemented with 10% FBS and 1% penicillin/streptomycin, plated in a T-75 tissue culture flask, and incubated at 37 °C in 5% CO_2. The medium was changed every two days. For experiments, 4×10^4 cells were seeded in a 35-mm culture dish with glass slides. After 24 h, the morphology of the cells was observed under a microscope.

Conflict of Interest: The authors declare no competing financial interest.

Acknowledgment. This work was supported by the Creative Research Initiatives research fund (project title: Smart Molecular Memory) of MEST/NRF

Supporting Information Available: Additional procedures, SEM images of PLL, images of bacterial growth in the presence of rGO, rGO–DS, and GO–DS, images of hAdSCs and A549 cell culture on GO–DS- and rGO–DS-coated coverslip, images of hAdSCs and A549 cell culture on PET, live/dead assay, BrdU assay and amount of nitrogen in different composites. This material is available free of charge *via* the Internet at http://pubs.acs.org.

Note Added after ASAP Publication: This paper was published online August 2, 2012. Corrections were made to Figures 6 and 7 and to Figures 3S and 4S in the Supporting Information, and the revised versions were reposted August 20, 2012.

REFERENCES AND NOTES

1. Geim, A. K.; Novoselov, K. S. The Rise of Graphene. *Nat. Mater.* **2007**, *6*, 183–191.
2. Yang, H.; Xia, Y. Bionanotechnology: Enabling Biomedical Research with Nanomaterials. *Adv. Mater.* **2007**, *19*, 3085–3087.
3. Yang, W.; Ratinac, K. R.; Ringer, S. P.; Thordarson, P.; Gooding, J. J.; Braet, F. Carbon Nanomaterials in Biosensors: Should You Use Nanotubes or Graphene? *Angew. Chem., Int. Ed.* **2010**, *49*, 2114–2138.
4. Chen, H.; Jiang, C.; Yu, C.; Zhang, S.; Liu, B.; Kong, J. Protein Chips and Nanomaterials for Application in Tumor Marker Immunoassays. *Biosens. Bioelectron.* **2009**, *24*, 3399–3411.
5. Xia, Y. Nanomaterials at Work in Biomedical Research. *Nat. Mater.* **2008**, *7*, 758–760.
6. Liu, H.; Webster, T. J. Nanomedicine for Implants: A Review of Studies and Necessary Experimental Tools. *Biomaterials* **2007**, *28*, 354–369.
7. Kim, J.; Kim, H. S.; Lee, N.; Kim, T.; Kim, H.; Yu, T.; Song, I. C.; Moon, W. K.; Hyeon, T. Multifunctional Uniform Nanoparticles Composed of a Magnetite Nanocrystal Core and a Mesoporous Silica Shell for Magnetic Resonance and Fluorescence Imaging and for Drug Delivery. *Angew. Chem., Int. Ed.* **2008**, *47*, 8438–8441.
8. Kim, J.; Piao, Y.; Hyeon, T. Multifunctional Nanostructured Materials for Multimodal Imaging, and Simultaneous Imaging and Therapy. *Chem. Soc. Rev.* **2009**, *38*, 372–390.
9. Chen, H.; Muller, M. B.; Gilmore, K. J.; Wallace, G. G.; Li, D. Mechanically Strong, Electrically Conductive, and Biocompatible Graphene Paper. *Adv. Mater.* **2008**, *20*, 3557–3561.
10. Agarwal, S.; Zhou, X.; Ye, F.; He, Q.; Chen, G. C.; Soo, J.; Boey, F.; Zhang, H.; Chen, P. Interfacing Live Cells with Nanocarbon Substrates. *Langmuir* **2010**, *26*, 2244–2247.
11. Park, S.; Mohanty, N.; Suk, J. W.; Nagaraja, A.; An, J.; Piner, R. D.; Cai, W.; Dreyer, D. B.; Berry, V.; Ruoff, R. S. Biocompatible, Robust Free-Standing Paper Composed of a TWEEN/Graphene Composite. *Adv. Mater.* **2010**, *22*, 1736–1740.
12. Ruiz, O. N.; Fernando, K. A. S.; Wang, B.; Brown, N. A.; Luo, P. G.; McNamara, N. D.; Vangsness, M.; Sun, Y.; Bunker, C. E. Graphene Oxide: A Nonspecific Enhancer of Cellular Growth. *ACS Nano* **2011**, *5*, 8100–8107.
13. Sondi, I.; Sondi, B. S. Silver Nanoparticles as Antimicrobial Agent: A Case Study on *E. coli* as a Model for Gram-Negative Bacteria. *J. Colloid Interface Sci.* **2004**, *275*, 177–182.
14. Lin, D. W.; Bettinger, C. J.; Ferreira, J. P.; Wang, C. L.; Bao, Z. A Cell-Compatible Conductive Film from a Carbon Nanotube Network Adsorbed on Poly-L-lysine. *ACS Nano* **2011**, *5*, 10026–10032.
15. Colville, K.; Tompkins, N.; Rutenberg, A. D.; Jericho, M. D. Effect of Poly(L-lysine) Substrate on Attached *Escherichia coli* Bacteria. *Langmuir* **2010**, *26*, 2639–2644.
16. Opatkiewicz, J. P.; LeMieux, M. C.; Bao, Z. Influence of Electrostatic Interactions on Spin-Assembled Single-Walled Carbon Nanotube Networks on Amine-Functionalized Surfaces. *ACS Nano* **2010**, *4*, 1167–1177.
17. Choi, E. Y.; Han, T. H.; Hong, J.; Kim, J. E.; Lee, S. H.; Kim, H. W.; Kim, S. O. Noncovalent Functionalization of Graphene with End-Functional Polymers. *J. Mater. Chem.* **2010**, *20*, 1907–1912.
18. Ghosh, D.; Chandra, S.; Chakraborty, A.; Ghosh, S. K.; Pramanik, P. A Novel Graphene Oxide-Para Amino Benzoic Acid Nanosheet as Effective Drug Delivery System to Treat Drug Resistant Bacteria. *Int. J. Pharm. Sci. Drug Res.* **2010**, *2*, 127–133.
19. Rozenberg, M.; Shoham, G. FTIR Spectra of Solid Poly-L-lysine in the Stretching NH Mode Range. *Biophys. Chem.* **2007**, *125*, 166–171.

20. Shan, C.; Yang, H.; Han, D.; Zhang, Q.; Ivaska, A.; Niu, L. Water-Soluble Graphene Covalently Functionalized by Biocompatible Poly-L-lysine. *Langmuir* **2009**, *25*, 12030–12033.
21. Ayala, P.; Grüneis, A.; Gemming, T.; Büchner, B.; Rümmeli, M. H.; Grimm, D. Influence of the Catalyst Hydrogen Pretreatment on the Growth of Vertically Aligned Nitrogen-Doped Carbon Nanotubes. *Chem. Mater.* **2007**, *19*, 6131–6137.
22. Compton, O. C.; Dikin, D. A.; Putz, K. W.; Brinson, C. L.; Nguyen, S. T. Electrically Conductive "Alkylated" Graphene Paper *via* Chemical Reduction of Amine-Functionalized Graphene Oxide Paper. *Adv. Mater.* **2010**, *22*, 892–896.
23. Long, D.; Li, W.; Ling, L.; Miyawaki, J.; Mochida, I.; Yoon, S. Preparation of Nitrogen-Doped Graphene Sheets by a Combined Chemical and Hydrothermal Reduction of Graphene Oxide. *Langmuir* **2010**, *26*, 16096–16102.
24. Li, D.; Muller, M. B.; Gilge, S.; Kaner, R. B.; Wallace, G. G. Processable Aqueous Dispersion of Graphene Nanosheets. *Nat. Nanotechnol.* **2008**, *80*, 101–105.
25. Shima, S.; Matsuoka, H.; Iwamoto, T.; Sakai, H. Antimicrobial Action of ε-Poly-L-lysine. *J. Antibiot.* **1984**, *37*, 1449–1455.
26. Krause, M.; Rösch, P.; Radt, B.; Popp, J. Localizing and Identifying Living Bacteria in an Abiotic Environment by a Combination of Raman and Fluorescence Microscopy. *Anal. Chem.* **2008**, *80*, 8568–8575.
27. Schäffler, A.; Büchler, C. Concise Review: Adipose Tissue-Derived Stromal Cells—Basic and Clinical Implications for Novel Cell-Based Therapies. *Stem Cells* **2007**, *25*, 818–827.
28. Park, S. Y.; Kim, Y. M.; Pyo, H. Gefitinib Radiosensitizes Non-small Cell Lung Cancer Cells through Inhibition of Ataxia Telangiectasia Mutated. *Mol. Cancer* **2010**, *9*, 222–234.
29. Leem, Y.; Han, J.; Lee, H.; Ha, H.; Kwon, Y.; Ho, S.; Kim, B.; Tran, P.; Bae, G.; Kang, J. Gas1 Cooperates with Cdo and Promotes Myogenic Differentiation *via* Activation of p38MAPK. *Cell. Signal.* **2011**, *23*, 2021–2029.
30. Tanaka, S.; Hayashi, T.; Tateyama, H.; Matsumura, K.; Hyon, S.; Hirayama, F. Application of the Bactericidal Activity of ε-Poly-L-lysine to the Storage of Human Platelet Concentrates. *Transfusion* **2010**, *50*, 932–940.
31. Moon, I. K.; Lee, J.; Ruoff, R. S.; Lee, H. Reduced Graphene Oxide by Chemical Graphitization. *Nat. Commun.* **2010**, *1*, 73–79.
32. Park, O. K.; Hahm, M. G.; Lee, S.; Joh, H.; Na, S.; Vajtai, R.; Lee, J. H.; Ku, B.; Ajayan, P. M. *In Situ* Synthesis of Thermochemically Reduced Graphene Oxide Conducting Nanocomposites. *Nano Lett.* **2012**, *12*, 1789–1793.